# 29.0 IDENTIFICATION OF DEFORMATION MECHANISMS IN THERMALLY STABLE CAST AL-CU ALLOYS *VIA* NEUTRON DIFFRACTION

Brian Milligan (Mines)
Faculty: Amy Clarke (Mines)
Industrial Mentor: Amit Shyam (ORNL), John Carpenter (LANL)

This project initiated in Fall 2017 and is supported by the Colorado School of Mines (Mines) and CANFSA, ORNL's Laboratory Directed Research and Development program, and the Higher Education Research Experiences program at Oak Ridge National Laboratory. The research performed during this project will serve as the basis for a Ph.D. thesis program for Brian Milligan.

## 29.1 Project Overview and Industrial Relevance

Cast Al-Cu alloys have long been popular in applications that require complex shapes, low density, and high strength. One such application is cylinder heads for internal combustion engines. However, as temperatures in commercial engines increase, the precipitates in these alloys begin to coarsen and transform during service. This leads to a loss of strength [29.1], due to a larger precipitate spacing [29.2], and a change in deformation mechanisms [29.3, 29.4].

Due to the anisotropy that arises during strain hardening in these alloys, an approach that takes orientation and phases into account is useful in studying their mechanical properties. These insights may be used to inform future efforts in alloy development and heat treating to improve properties such as ductility and fatigue performance.

## 29.2 Previous Work

### 29.2.1 Literature Review

Al-Cu precipitation has been studied in detail and generally follows the transformation pathway: supersaturated solid solution → plate-shaped, single atomic layer Guinier-Preston (GP) I zones → plate-shaped, 2-4 layer GPII/θ″ precipitates → thick, plate shaped θ′ precipitates → approximately spherical or rod-shaped θ equilibrium precipitates [29.2]. This range of precipitate sizes, morphologies, and structures leads to a large difference in mechanical properties with even small differences in aging treatments of Al-Cu alloys. The effect of precipitate structure on mechanical properties has long been a popular area of study [29.5]. With modern computational tools and experimentation, models to describe these quantities are being continually refined. Of particular interest is the work of da Costa Teixiera *et al.*, who have improved the accuracy yielding and strain hardening model for Al-Cu alloys by omitting the common assumption of spherical precipitates [29.3, 29.4].

The studies mentioned above have mostly looked at mechanical behavior of precipitate strengthened alloys in a bulk, continuum manner. Recently, however, there has been significant interest in the precipitate-dislocation interactions at an individual precipitate scale, as these interactions are important in determining strain hardening behavior. While this has been discussed for quite some time and predictions have been made for the precipitates to undergo extremely high stresses due to coherency requirements with the matrix (similar to an oxide strengthened metal matrix composite [29.6]), there hasn't been experimental or modeling techniques capable of determining whether the precipitates could sustain such stresses [29.7]. Modern techniques have recently allowed for the study of these precipitates individually, which have provided powerful insights into their behavior. Two such studies come from Krasnikov *et al.* and Kaira *et al.*, whom have studied the shearing behavior of θ′ precipitates using dislocation dynamics and atomistic simulations and 4-D X-ray imaging methods, respectively [29.8, 29.9]. These studies corroborate with the bulk modeling by da Costa Teixeira *et al*, all three of which predict that precipitates will be bypassed by dislocations at the yield of the bulk material, later being sheared by dislocations in a process referred to as delayed shearing, as shown schematically in **Figure 29.1 (a-c)**.

### 29.2.2 Identification of Deformation Mechanisms *via* Neutron Diffraction

In-situ neutron diffraction was applied to Al alloy 206 (composition shown in **Table 29.1**) with four different aging conditions, corresponding to four different precipitate structures. The aging conditions and precipitate structures of the three most relevant aging treatments are shown in **Table 29.2** and **Figure 29.2**, respectively. Due to their

intertwined nature, the results from the matrix and precipitates will be discussed together in the next section of this report. Modeling was also done on the orientation-dependent nature of strain hardening in the matrix; the strain hardening rate was found to depend on the orientation of the precipitate slip planes relative to the applied stress. For further detail, refer to B. Milligan's Spring 2019 CANFSA report.

## 29.3 Recent Progress

### 29.3.1 Identification of Stresses in Precipitate Phases

Due to their low phase fraction, the neutron diffraction peaks in the precipitate phases in 206 are relatively difficult to measure. In order to remedy this, a very long measurement time was used. However, using a long measurement time would normally reduce the number of data points to such a degree that relevant information would be difficult to extract from the data. Therefore, an overlapping time scheme was used where measurements were taken for 20 minutes, spaced 5 minutes apart. Even using this technique, the precipitate diffraction peaks were small (**Figure 29.3**). Fortunately, the precipitate phases displayed extremely high lattice strains, and useful information was still extracted.

**Figure 29.4** shows the lattice strain results for various orientations of both the precipitate and matrix phases. Lattice strain is internal elastic strain within a particular orientation and phase, measured by the stretching of lattice planes. Plots on the left half display lattice strain versus applied stress. Since lattice strain only measures elastic effects, it depends linearly on the internal stress, and therefore this plot would show a straight line for a single crystal. However, stress can be transferred from one phase or grain to other phases or grains, and stress transfer can be seen in the 200°C and 300°C overaged conditions after the yield point of the material. Curves that stray left of the straight line (which represents the average lattice strain for the bulk material) are transferring stress to surrounding grains or precipitates, while curves that stray right are accepting stress from their surroundings. The mechanism that allows this is similar to the behavior of a ceramic-reinforced metal matrix composite. The weak matrix yields before the precipitate, and due to coherency requirements of the precipitate, the precipitate must undergo the same amount of elastic strain as the plastic strain of the matrix. The high elastic strains in the precipitates translates to high stresses in the precipitates.

On the right half of **Figure 29.4**, lattice strain is shown as a function of measured external strain. Since lattice strain is only elastic, this plot essentially acts as an orientation- and phase-specific stress-strain curve. It also displays an important effect in the precipitate behavior, where after a certain amount of strain in the bulk, the lattice strain (which was increasing quickly) flattens out. This is evidence for the precipitates yielding, as was previously predicted by multiple authors [29.3, 29.4, 29.7-29.9]. In the 200°C overaged condition, the precipitate likely yields from the delayed shearing mechanism, while in the 300°C overaged condition (**Figure 29.1**), the precipitate likely "yields" by cracking. In the 200°C overaged condition, only one of the two observed precipitate orientations appear to yield during the test. This suggests that there is anisotropy in the behavior of the θ′ precipitates, while the θ precipitates both begin to crack at around the same measured external strain.

The anisotropy in the precipitate behavior in the 200°C overaged condition will translate to anisotropy in the strain hardening behavior of the matrix, which is also displayed in **Figure 29.4**. The stages of deformation in the precipitates and matrix are displayed schematically in **Figure 29.5**. Precipitate shearing is a strain softening mechanism, while Orowan looping is a hardening mechanism, so grains which contain precipitates that are shearable will have a lower strain hardening rate than grains that have non-shearable precipitates. The degree of shearability of the precipitates, found previously to depend on the orientation of the precipitates' slip planes relative to the applied stress (**Figure 29.1**), was modeled using interface energy, and the interfacial energy was found to have a positive relationship with strain hardening rate of the matrix. For further detail, refer to B. Milligan's Spring 2019 CANFSA report.

## 29.4 Plans for Next Reporting Period

- Perform additional TEM on 206 Al to observe sheared precipitates.
- Continue analysis on alloy RR350 to study strain hardening as a function of temperature.
- Submit prepared publication on the results outlined in this document to Acta Materialia.
- Respond to requested changes on MSEA paper on creep of Al-Cu alloys.

## 29.5 References

[29.1] S. Roy, L.F. Allard, A. Rodriguez, W.D. Porter, A. Shyam, Comparative Evaluation of Cast Aluminum Alloys for Automotive Cylinder Heads: Part II—Mechanical and Thermal Properties, Metallurgical and Materials Transactions A. 48 (2017) 2543–2562.

[29.2] S. Roy, L.F. Allard, A. Rodriguez, T.R. Watkins, A. Shyam. Comparative Evaluation of Cast Aluminum Alloys for Automotive Cylinder Heads: Part I—Microstructure Evolution, Metallurgical and Materials Transactions A. 48 (2017) 2529–2542.

[29.3] J. da Costa Teixeira, D.G. Cram, L. Bourgeois, T.J. Bastow, A. J. Hill, C. R. Hutchinson, On the strengthening response of aluminum alloys containing shear-resistant plate-shaped precipitates, Acta Materialia. 56 (2008) 6109-6122.

[29.4] J. da Costa Teixeira, L. Bourgeois, C.W. Sinclair, C.R. Hutchinson, The effect of shear-resistant, plate-shaped precipitates on the work hardening of Al alloys: Towards a prediction of the strength–elongation correlation, Acta Materialia. 57 (2009) 6075-6089.

[29.5] A.J. Ardell, Precipitation Hardening, Metallurgical Transactions A 16 (1985) 2131-2165

[29.6] N. Shi, M.A.M Bourke. J.A. Roberts, J.E. Allison, Phase-Stress Partitioning during Uniaxial Tensile Loading of a TiC-Particle-Reinforced Al Composite, Metallurgical and Materials Transactions A. 28 (1997) 2741-2753

[29.7] A. Kelly, R.B. Nicholson, Precipitation Hardening, Progress in Materials Science 10 (1963) 149-391

[29.8] V.S. Krasnikov, A.E. Meyer, Dislocation dynamics in aluminum containing θ′ phase: Atomistic simulation and continuum modeling, International Journal of Plasticity 119 (2019) 21-42.

[29.9] C.S. Kaira *et al*, Microstructural evolution and deformation behavior of Al-Cu alloys: A Transmission X-ray Microscopy (TXM) and micropillar compression study, Acta Materialia 144 (2018) 419-431.

## 29.6 Figures and Tables

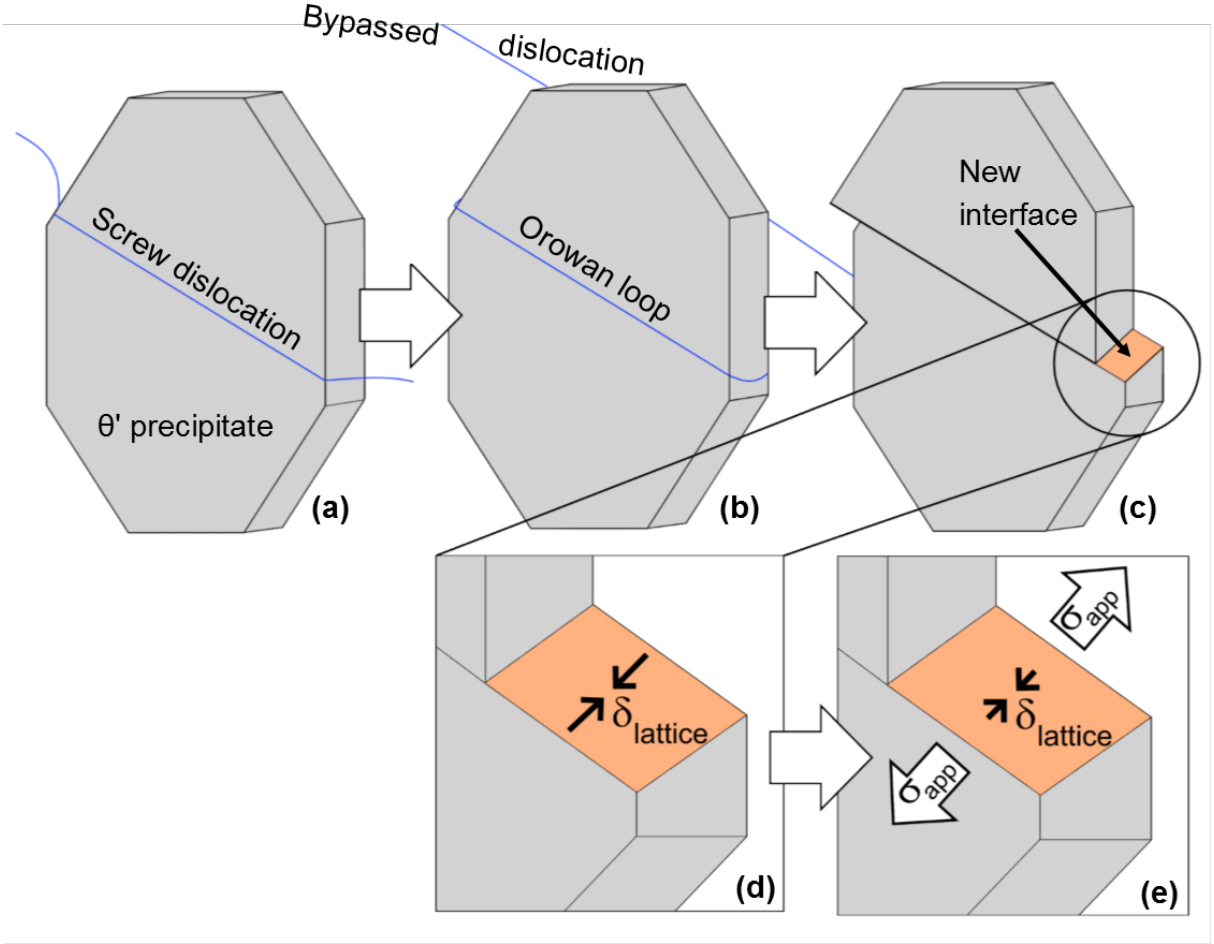


Figure 29.1: Schematic of the delayed shearing process. The steps are as follows: (a) A dislocation meets the precipitate. (b) The stress is high enough that the dislocation bypasses the precipitate *via* Orowan looping. (c) The previous step repeats multiple times, and the local stress becomes high enough that the precipitate shears. This shearing process is orientation-dependent; if the applied stress is oriented in such a way that it opposes the interface misfit on the shear plane, the energy required to shear the precipitate is reduced (d,e).

Table 29.1: Composition of Al alloy 206, in weight percent.

| Cu | Mg | Mn | Fe | Si | Ti | Al |
|---|---|---|---|---|---|---|
| 4.5 | 0.30 | 0.23 | 0.14 | 0.12 | 0.02 | Bal. |

Table 29.2: Description of the heat treatments applied prior to neutron diffraction analysis. OA stands for overage.

| Condition | Solutionize | Quench | Peak Age | Overage |
|---|---|---|---|---|
| Natural Age | 530°C for 5hr | 80-90°C in water | None | None |
| 200°C OA | | | 190°C for 5h | 200°C for 200 h |
| 300°C OA | | | | 300°C for 200 h |

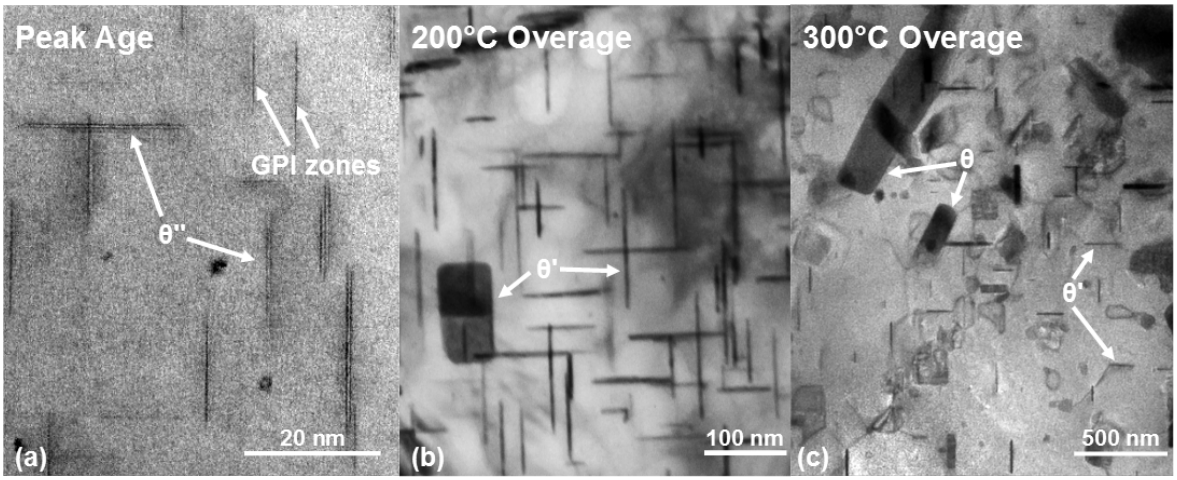


Figure 29.2: Precipitate structure of Al alloy 206 under three aging conditions (which are described in **Table 29.1**). Note the difference in scale across the three images.

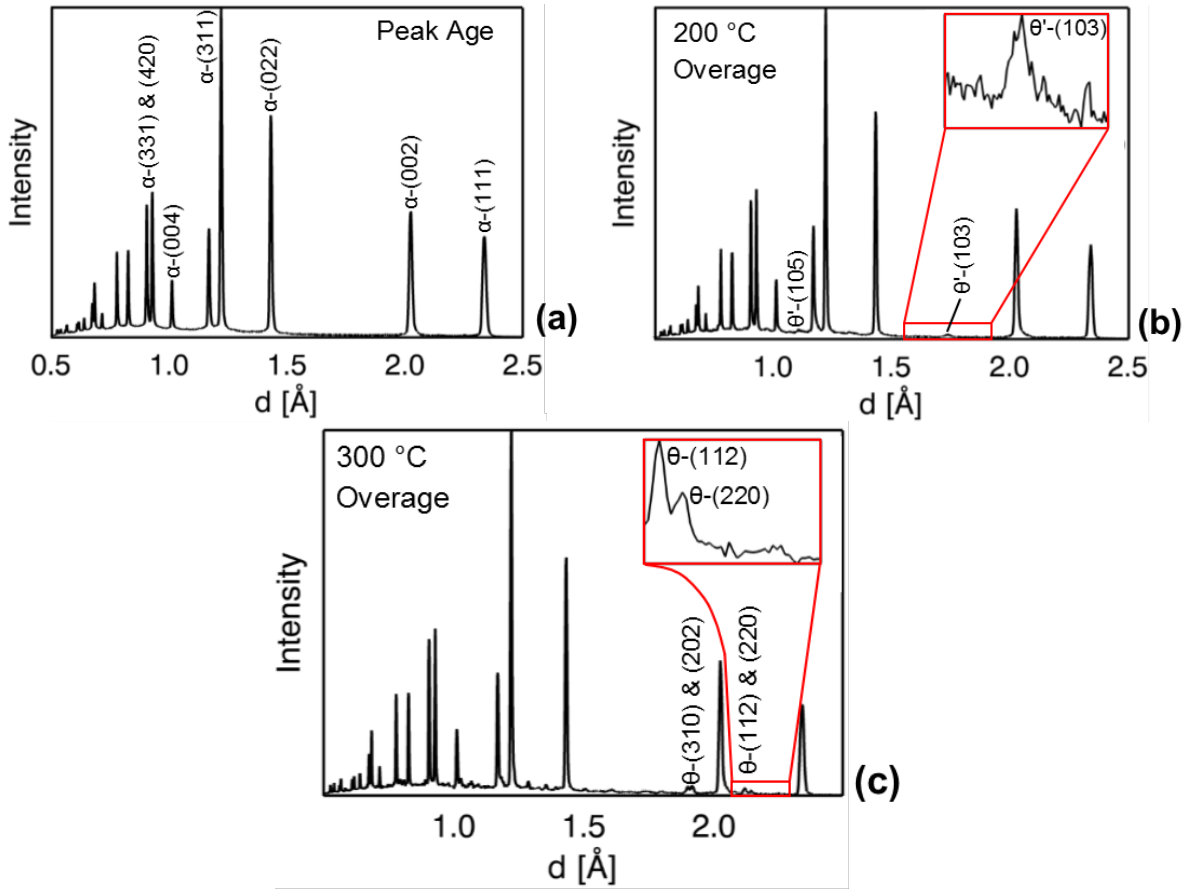


Figure 29.3: Neutron diffraction patterns collected during tensile loading, highlighting the precipitate peaks. Peaks that will be discussed later are labelled with their phase and the Miller indices of their corresponding lattice planes.

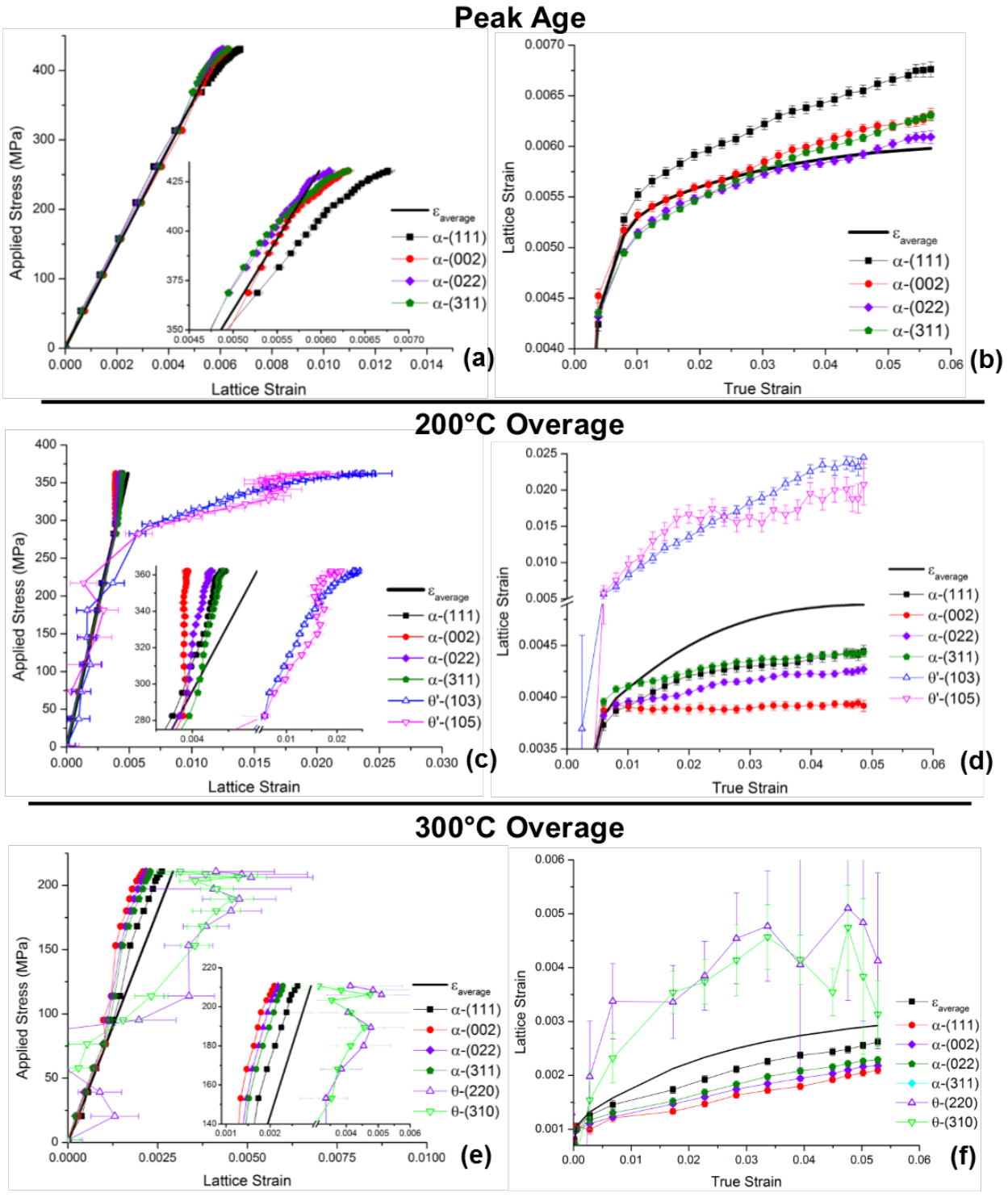


Figure 29.4: Lattice strain measurements taken during tensile loading compared against applied stress (a, c, e) and true strain measured with an extensometer (b, d, f) for each aging condition.

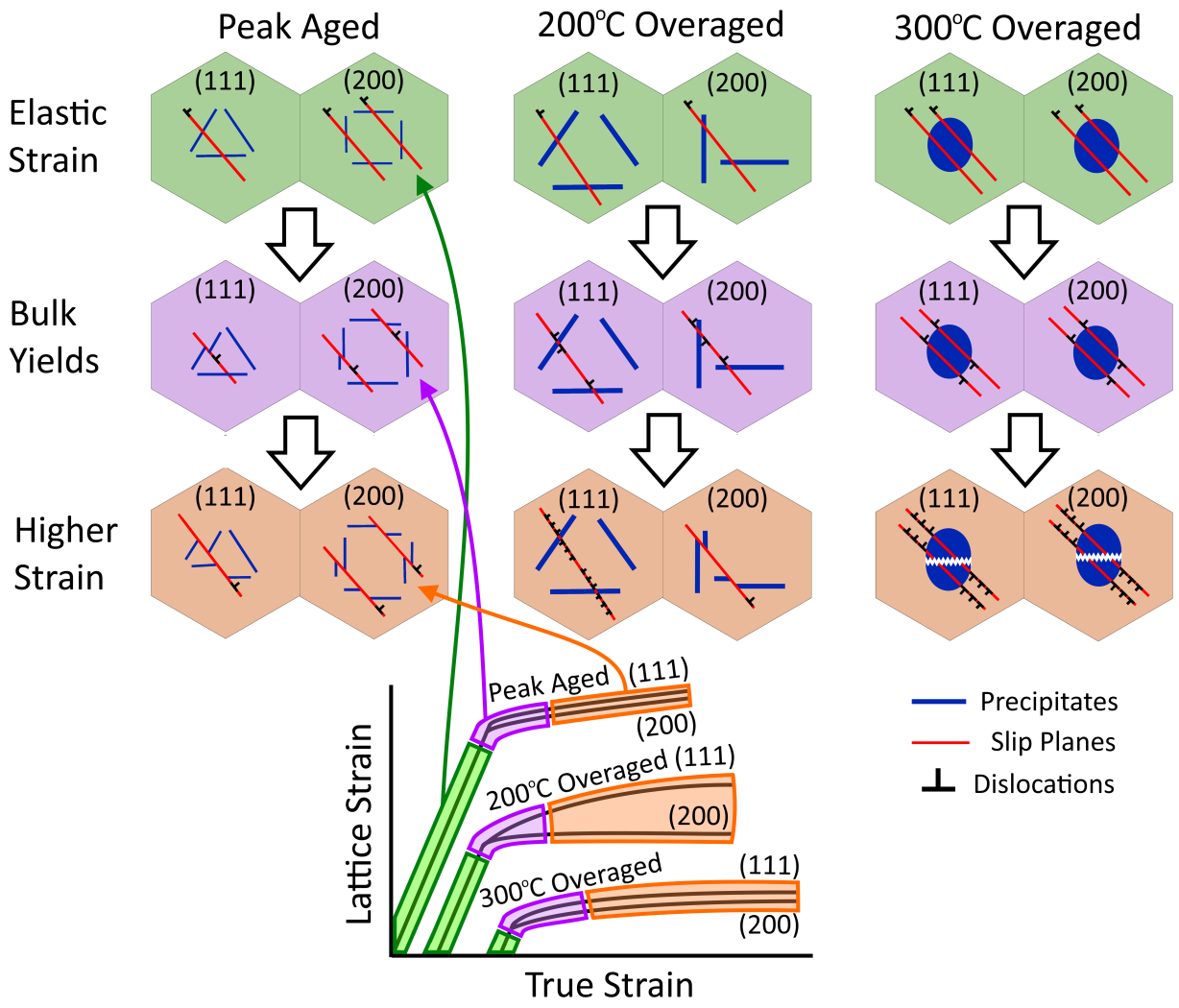


Figure 29.5: Schematic representation of the different stages of tensile loading. The test begins with elastic loading, during which each aging condition acts in a fairly similar way. Dislocations have not moved far, and no bypassing events have occurred. Next, the bulk material yields. In the peak aged condition, this is due to precipitate shearing (since the precipitates in this condition are small and coherent), while in the 200°C and 300°C overaged conditions Orowan looping occurred instead. At higher strain, shearing continues in the peak aged condition, while in the 200°C overaged condition, some precipitates sheared while some continued to undergo Orowan looping (depending on their orientation). This leads to anisotropy that can be observed in the bulk. In the 300°C overaged condition, the precipitates begin to crack at high strain. Note that GP I and GP II/θ″ zones exist in the peak aged condition, θ′ precipitates exist in the 200°C overaged condition, and θ equilibrium precipitates exist in the 300°C overaged condition.